Materials Today Bio 23 (2023) 100833

Contents lists available at ScienceDirect

Materials Today Bio

journal homepage: www.journals.elsevier.com/materials-today-bio

3D-printed PCL scaffolds with anatomy-inspired bionic stratified structures for the treatment of growth plate injuries

Xianggang Wang [a,b], Zuhao Li [a,b], Jiaqi Liu [a,b], Chenyu Wang [c], Haotian Bai [a,b], Xiujie Zhu [a,b], Hui Wang [a,b], Zhonghan Wang [a,b], He Liu [a,b,*], Jincheng Wang [a,b]

[a] Orthopaedic Medical Center, The Second Hospital of Jilin University, Changchun, 130041, PR China
[b] Orthopaedic Research Institute of Jilin Province, Changchun, 130041, PR China
[c] Department of Plastic and Reconstructive Surgery, The First Hospital of Jilin University, Changchun, 130021, PR China

ARTICLE INFO

Keywords:
Growth plate injury
3D printing
Bionic stratified scaffold
Cartilage tissue engineering
Chondrogenesis

ABSTRACT

The growth plate is a cartilaginous tissue with three distinct zones. Resident chondrocytes are highly organized in a columnar structure, which is critical for the longitudinal growth of immature long bones. Once injured, the growth plate may potentially be replaced by bony bar formation and, consequently, cause limb abnormalities in children. It is well-known that the essential step in growth plate repair is the remolding of the organized structure of chondrocytes. To achieve this, we prepared an anatomy-inspired bionic Poly(ε-caprolactone) (PCL) scaffold with a stratified structure using three-dimensional (3D) printing technology. The bionic scaffold is engineered by surface modification of NaOH and collagen I (COL I) to promote cell adhesion. Moreover, chondrocytes and bone marrow mesenchymal stem cells (BMSCs) are loaded in the most suitable ratio of 1:3 for growth plate reconstruction. Based on the anatomical structure of the growth plate, the bionic scaffold is designed to have three regions, which are the small-, medium-, and large-pore-size regions. These pore sizes are used to induce BMSCs to differentiate into similar structures such as the growth plate. Remarkably, the X-ray and histological results also demonstrate that the cell-loaded stratified scaffold can successfully rebuild the structure of the growth plate and reduce limb abnormalities, including limb length discrepancies and angular deformities *in vivo*. This study provides a potential method of preparing a bioinspired stratified scaffold for the treatment of growth plate injuries.

1. Introduction

The growth plate, also known as the physis, is the cartilaginous area that exists at the near end of immature long bones. It is mainly responsible for the longitudinal growth of children as the elongation of long bones by endochondral ossification mainly occurs there [1]. As a cartilaginous region, the growth plate is vulnerable to injuries such as fractures, infection, or tumors. Approximately 15–30 % of pediatric traumas involve the growth plate [2]. In clinical practice, the fractures of the growth plate are divided into five categories per the Salter-Harris (SH) Classification System. Among the five types, those that cross the growth plate (types III and IV) and the compression type (type V) are more likely to cause bony bar formation, which will result in growth arrest [3,4]. Patients with severe injuries require surgical resection of the bony bar and the insertion of interpositional materials. However, this surgical procedure often leads to limb-length discrepancy and angular deformity [5]. Thus, it is urgent to find a new strategy for growth plate reconstruction.

In recent years, tissue engineering approaches are considered promising strategies for the treatment of growth plate injuries. Key factors for tissue engineering technologies include proper biomaterials, suitable cells, and bioactive substances to induce chondrogenesis [6]. However, the lack of a blood-vascular system in the growth plate limits cell viability in regenerative strategies [7]. There is a critical need to prepare a tissue-engineered growth plate capable of acting as an endogenous production workshop for chondrocyte regeneration and cartilaginous ECM deposition. As for the proper biomaterial, nowadays, lots of biomaterials with good biocompatibility and degradability are used in cartilage tissue engineering; these include Poly(ε-caprolactone) polymer (PCL), Poly(lactic-co-glycolic acid) (PLGA), Polylactic acid (PLA), silk, and alginate [8]. Among these biomaterials, PCL is one of the most widely used in cartilage tissue engineering [9]. PCL, a

* Corresponding author. Orthopaedic Medical Center, The Second Hospital of Jilin University, Changchun, 130041, PR China.
E-mail address: heliu@jlu.edu.cn (H. Liu).

https://doi.org/10.1016/j.mtbio.2023.100833
Received 23 April 2023; Received in revised form 27 July 2023; Accepted 14 October 2023
Available online 19 October 2023

semi-crystalline aliphatic polyester, is widely used in tissue engineering as a hydrophobic biological biomaterial [10]. Thanks to its brilliant biocompatibility and thermoplasticity, PCL is one of the most suitable materials for 3D printing [11]. Moreover, it is also degradable and can be manufactured with various drugs and growth factors. It is reported that its high molecular weight is associated with its slow degradation rate. PCL is an excellent biomaterial for making scaffolds in cartilaginous tissue engineering [12]. However, the hydrophobicity of PCL makes it difficult for it to adhere to cells. To solve this issue, in previous studies, various strategies have been used to modify the PCL surface to enhance cell adhesion. These strategies include polydopamine coating [13], COL IV coating [14], arginylglycylaspartic acid (RGD) immobilization [15], and plasma modification [16]. All these modifications performed using proteins are expensive and complicated. Nowadays, NaOH corrosion and COL I coating have proven to be a much easier and more economic strategy. After NaOH corrosion, the smooth surfaces of

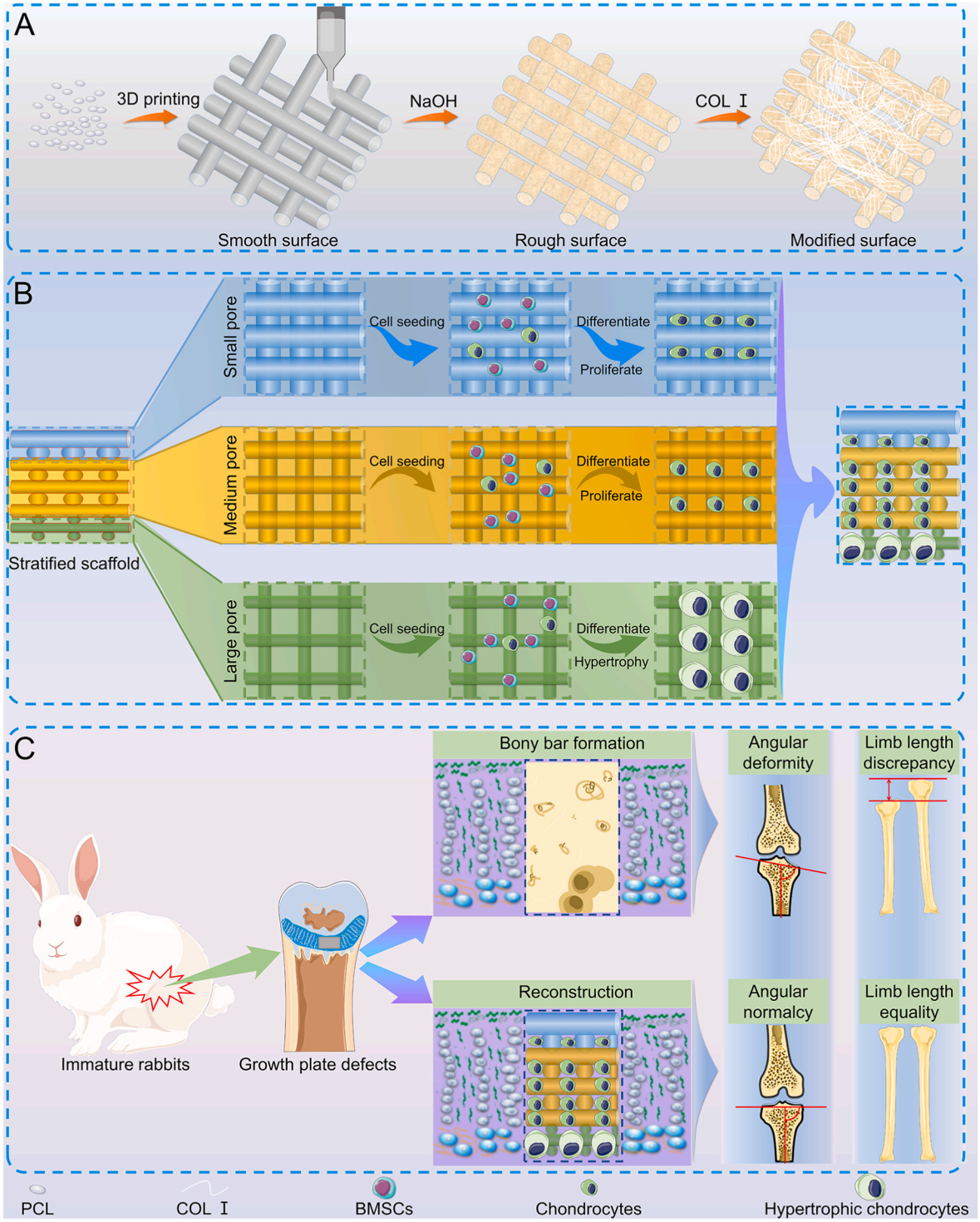

Scheme 1. Schematic illustration of the tissue-engineered scaffold and its therapeutical effect on growth plate injuries. (A) Surface modification of the 3D-printed PCL scaffolds. (B) Effect of chondrogenic differentiation on the co-culture of chondrocytes and BMSCs in different pore sizes. (C) The therapeutic effect of tissue-engineered scaffolds for the treatment of growth plate injuries.

PCL scaffolds became rougher. The irregular surface improves the hydrophilicity of the PCL surface [17]. Moreover, COL I has been widely used in making hydrogels in tissue engineering, considering its excellent water absorption [18]. COL I coating will further improve the hydrophilicity of PCL scaffolds. Therefore, both NaOH corrosion and COL I coating are effective for PCL surface modification.

Besides the selection and modification of suitable biomaterials, many studies have also found that parameters of scaffolds, including the pore size, fiber thickness, and roughness, play important role in cell adhesion, proliferation, and differentiation [19]. As for chondrocytes, the pore size will significantly affect cell proliferation and gene expression. It is rational to use stratified scaffolds with gradient pore sizes to induce the development of chondrogenesis-like chondrocytes in the growth plate. However, there is a paucity of such studies in previous research. Meanwhile, articular cartilage has a highly organized cartilaginous structure similar to that of the growth plate, and many studies have investigated the effects of stratified scaffolds with different pore sizes for articular cartilage repair [20,21]. These studies have demonstrated that, compared to scaffolds with a single pore size, the stratified scaffold with gradient pore sizes is a more promising tool for chondrogenesis and can be considered for cartilage tissue engineering applications [22,23]. Therefore, more studies are needed to elucidate the effect of stratified scaffolds with different pore sizes for the treatment of growth plate injuries.

In this study, we used the 3D printer of the Fused Deposition Modeling to make a delicate scaffold with a bionic stratified structure for growth plate reconstruction. The scaffold had three distinct regions, which were the small-pore-size (88.05 ± 7.32 μm) region, the medium-pore-size (224.35 ± 7.05 μm) region, and the large-pore-size (404.18 ± 26.98 μm) region. We hypothesized that the small- and medium-pore-size regions would induce chondrocyte proliferation and ECM secretion. The large-pore-size region would promote the transformation of chondrocytes to hypertrophic chondrocytes, just like cell behavior in the hypertrophic zone (Scheme 1).

2. Materials and methods

2.1. Materials

The poly(ε-caprolactone) polymer (PCL) (Mw = 80000) was purchased from Rhawn, (Shanghai, China). The double-distilled water used in all experiments was obtained from a Milli-Q A10 filtration system (Millipore, Billerica, MA, USA). The low-glucose Dulbecco's Modified Eagle's Medium (LG-DMEM), high-glucose Dulbecco's Modified Eagle's Medium (HG-DMEM), Dulbecco's Modified Eagle's Medium/Ham's F12 (DMEM/F12), streptomycin–penicillin, and fetal bovine serum (FBS) were purchased from Gibco Life Technologies (Grand Island, NY, USA). The 4 % paraformaldehyde solution, phosphate-buffered saline (PBS), and COL I were purchased from Solarbio (Beijing, China). The Live-Dead staining kit was purchased from Bioss (China) and the Cell Counting Kit-8 (CCK-8) was purchased from Beibo (Beijing, China). The Hematoxylin and Eosin (H&E) stain, Van Gieson (VG) stain, and Masson's trichrome were obtained from Thermo Fisher Scientific (Shanghai, China). Modified Saffron-O and Fast Green Stain Kit were purchased from Solarbio (Beijing, China). COL II and COL X antibodies were purchased from Bioss (Beijing, China). Osteocalcin (OCN) antibodies were purchased from GeneTex (SC, USA).

2.2. Fabrication of stratified PCL scaffolds

The bioinspired bionic scaffolds were prepared via FDM techniques using a single nozzle. Briefly, PCL (molecular weight: 80000) particles were loaded into the material cylinder for heat-melting. The nozzle temperature was set at 120 °C while the printing bed was 40 °C. The volume of the model was 30 × 30 × 2 mm^3. The printing fibers were predesigned layer by layer, and the thickness of each layer was 0.2 mm. The porosity of the scaffolds was predesigned at 40 %. There were ten layers in every scaffold. Scaffolds with varying pore sizes were achieved by changing the printing speed for each layer. The printing speed for the first two layers was 6 mm/s, that for layers 3–7 was 12 mm/s, and that for the last three layers was 18 mm/s. To meet the experimental needs after finishing the stratified scaffolds, the final volume for cell experiments was 10 × 10 × 2 mm^3, and it was 5 × 5 × 2 mm^3 *in vivo*.

The pore sizes of the scaffolds in each layer were observed using a light microscope. The pore sizes and string sizes were calculated from the images. The elastic modulus, compression modulus, and tensile modulus of the stratified scaffold and every region were measured using the AG-A20 KNA dynamic testing machine (Shimadzu, Nakagyo-ku, Kyoto, Japan).

2.3. Cell isolation

Bone marrow mesenchymal stem cells (BMSCs) were isolated from healthy one-week-old New Zealand white rabbits as previously described [24]. Briefly, BMSCs were cultured in LG-DMEM containing 10 % PBS and 1 % streptomycin-penicillin. The cells were placed in a humidified incubator at 5 % CO_2 and at 37 °C. The medium was changed every three days. BMSCs were digested and passaged only when they reached 70–80 % confluence. BMSCs after the second generation were qualified for further experiments. Chondrocytes were isolated from articular cartilage. The cartilages were minced to 1 × 1 × 1 mm, washed three times with PBS, and digested with 0.2 % collagenase type II overnight. After centrifugation, the chondrocytes were collected and cultured in HG-DMEM with 10 % FBS and 1 % penicillin-streptomycin at 5 % CO_2 and 37 °C. They were prepared for further experiments after two passages.

2.3.1. Preparation of the modified scaffolds and their cell viability

The hydrophobicity of the PCL material rendered it unsuitable for cell adhesion. To find an effective strategy for PCL scaffold surface modification, we compared the effects of PCL scaffolds with three different modifications. The three strategies were as follows:

1) Single poly-D-lysine coating: The PCL scaffolds were placed in the 12-well palates. Scaffolds were sterilized by spraying them with 75 % alcohol and irradiating them (front and back) with ultraviolet rays for 60 min. Finally, 2 ml of 50 μg/ml poly-D-lysine was used to immerse the scaffolds for 8 h.
2) NaOH soaking: The 3D-printed stratified scaffolds were immersed in 3 M NaOH for 24 h.
3) COL I coating after NaOH soaking: After treatment with NaOH 24 h, 50 μl 5 mg/ml COL I was used for scaffold surface coating. All the scaffolds were washed three times using PBS before cellular experiments.

A live/dead assay was used to test the cell viability of the modified scaffolds. Briefly, BMSCs were seeded on the modified scaffolds at a density of 2 × 10^4 cells/well in 24-well plates. After incubation for three days at 37 °C and 5 % CO_2, the scaffolds were immersed in 1 mM Calcein-AM solution for 30 min and then stained using 1 μg/ml PI for 5 min. All the processes were performed in dark environments and carried out per the manufacturer's protocol. In the end, the results were imaged via fluorescence microscopy (Olympus IX71, Tokyo, Japan).

2.4. Cell morphology of the modified scaffolds

The modification of COL I showed the best results for cell adhesion through the live/dead assay. To evaluate the cell morphology of the modified scaffolds, we performed rhodamine-phalloidin staining. BMSCs were seeded on scaffolds' free wells and the COL I-modified scaffolds at a density of 1 × 10^4 cells/well in 24-well plates. The cells were cultured for one day before the morphological assessment. The

samples were fixed with 4 % paraformaldehyde for 10 min. Then, BMSCs were permeabilized with 0.5 % Triton X-100 solution for 5 min. After repeated washing with PBS, the cells were stained with 100 nM rhodamine-phalloidin for 30 min, followed by 100 nM DAPI staining for 1 min. Finally, images were captured via fluorescence microscopy.

2.5. Topographic characterization of the scaffolds with or without surface modification

The morphologies of the original 3D-printed bionic stratified scaffolds, NaOH-treated scaffolds, and COL I-modified scaffolds were observed using a JEOL JSM-67OOF scanning electron microscope (SEM). The water contact angle measurement was performed using a VCA optima XE contact angle system. The testing environment was set at 25 °C and 48 % humidity. The volume of each water droplet was approximately 2 μl. Each droplet was carefully attached to the surface of the scaffolds and recorded by a charge-coupled device camera. The process of water contact angle measurement for each modified surface was repeated three times. The calculation of the water contact angle was performed using Image J software, and the average value for each sample was represented.

2.6. Cell proliferation of the chondrocytes and BMSCs co-culture

The CCK-8 experiment was performed to evaluate the proliferation rate of the co-culture of chondrocytes and BMSCs. The cells were seeded in the COL I- and NaOH-modified scaffolds in 24-well plates at a total density of 3×10^4 cells/well. The groups were identified according to the co-culture ratio of chondrocytes and BMSCs. They were divided into the 0:1, 3:1, 2:1, 1:1, 1:2, 1:3, and 0:1 groups. The CCK-8 assay was performed 1, 4, and 7 days after cell seeding. At every given time point, the CCK-8 solution was used to count the cells in each well. After 2 h of incubation, the reaction solution was transferred to a 96-well plate, and OD values were read using a microplate reader at 450 nm. The proliferative ratios were calculated based on OD values on day 1.

2.7. Induced chondrogenic differentiation of the co-culture of chondrocytes and BMSCs

To study the chondrogenic ability of the co-culture of chondrocytes and BMSCs, 6×10^4 cells/well (chondrocytes and BMSCs) were seeded on 12-well plates in different ratios. The medium was changed every three days. After seven and fourteen days of co-culture, the secretion of glycosaminoglycan (GAG) and COL II was measured using the GAG ELISA and COL II ELISA kits. The process was conducted per the manufacturer's protocol. Briefly, the culture supernatant of co-cultured cells (10 μl, diluted in a 1:200 ratio) and 100 μl of horseradish peroxidase (HRP) conjugated secondary antibodies were added to the precoated 96-well plates. The plates were incubated at 37 °C for 60 min. After washing five times, 50 μl of the tetramethylbenzidine (TMB) substrate and 50 μl of the corresponding buffer were added to each well. Then the plates were incubated at 37 °C for 15 min. After incubation, the reaction was stopped by adding 50 μl of sulfuric acid solution to the mixture. Finally, the OD values at 450 nm were measured, and concentrations of the proteins were calculated according to the standard curves.

Similarly, after 14 days of co-culture, the cells on the scaffolds were fixed with 4 % paraformaldehyde for 10 min. Then, PBS washing was repeated three times. Staining was performed using Alcian blue dye for 10 min, after which the samples were washed with PBS again before observation under a light microscope.

2.8. Chondrogenic differentiation in three distinct regions of the scaffolds

In vitro immunofluorescence staining of cells and Safranin O and Fast Green staining were employed to evaluate the expression of chondrogenic-related proteins within the three distinct regions of the scaffolds. The cellular ratio of chondrocytes to BMSCs was 1:3, and the total number of cells in each 12-well plate was 6×10^4. After co-culture for 14 days, the cells were fixed with 4 % paraformaldehyde for 10 min. For the Safranin O and Fast Green staining, samples were immersed in 0.1 % Fast Green solution for 5 min. After staining, the sections were washed with distilled water to remove any unbound dye. Subsequently, the samples were incubated in 0.1 % Safranin O solution (pH 5.0) for 5 min at room temperature. The excess stain was gently rinsed off with distilled water before observing the results.

For immunohistochemical staining, following fixation with formalin, they were permeabilized by applying 0.5 % Triton X-100 for 5 min and blocked by applying 3 % BSA for 30 min. Thereafter, the cells were treated with primary antibodies of COL II and COL X at 4 °C overnight. Subsequently, they were incubated by secondary antibodies for 1 h. The results were observed via fluorescence microscopy, and the relative fluorescence intensity in each region was calculated using Image J software.

The chondrogenic differentiation of chondrocytes and BMSCs co-culture at different regions of the scaffolds was also tested via RT-qPCR. The cellular ratio of chondrocytes to BMSCs was 1:3, and the total number of cells in each 6-well plate was 12×10^4. After incubation for 7 and 14 days, the expression of the chondrogenesis-related genes (*aggrecan* and *Sox-9*) was investigated. The primer sequences of the genes are displayed in Table S1.

2.9. Preparation of the growth plate defect models and scaffold implantation

All animal experimental protocols were in accordance with the guidelines of the Animal Care and Use Ethics Committee of Jilin University. Forty-eight three-week-old male New Zealand rabbits were randomly divided into four groups. All the animals were allowed to acclimatize for one week before surgery, and they had access to water and food ad libitum. The rabbits were anesthetized using 3 % pentobarbital sodium at a dose of 50 mg/kg. The surgical area was carefully shaved and sterilized before it was placed on the surgical table. A 3-cm-long anterior-medial longitudinal incision was made near the medial side of the right tibial tubercle as described [25]. The growth plate was identified as a white line of tissue between the distal insertion of the medial collateral ligament and the tibial tubercle. A 2-mm-wide burr was installed in a rotary tool. The drilling depth was controlled and limited to 5 mm by a plastic stopper on the burr. Growth plate defects were parallel to the joint line and perpendicular to the tibial shaft. Then, a $5 \times 5 \times 2$ mm growth plate defect (25 %) was achieved. The scaffolds were implanted according to the following treatment groups: 1) the control group (without scaffolds); 2) 3D printed scaffolds with uniform pore sizes; 3) 3D printed scaffolds with stratified pore sizes (the small-pore-size region was close to the joint cavity while the large-pore-size region was at the distal end of the defect); 4) 3D-printed stratified scaffolds containing chondrocytes and BMSCs (cell ratio: 1:3; total cell number: 6×10^4 cells per scaffold). The incision was stitched layer by layer with absorbable sutures. After surgery, all the animals were injected with penicillin for three days to prevent infection. They were kept in separate cages and allowed free movement. Eight weeks and 28 weeks after surgery, the rabbits were sacrificed for evaluation.

2.10. Radiography of the animals

To assess the angular deformity and limb length discrepancy in different groups, the rabbits were imaged with an X-ray apparatus (Houhua GDX-75Y, Xian, China) before sacrifice. Pictures of the left and right knee joints in the antero-posterior view were collected. Angles of the deformity were measured and limb length discrepancies were calculated.

2.11. Histological examination

Proximal tibias were collected from all animals. The tibial samples were fixed in 4 % formaldehyde and demineralized for six weeks using a 10 % Ethylene Diamine Tetra-acetic Acid (EDTA) solution. Then, the samples were dehydrated and embedded in paraffin. Each region of interest (ROI) was cut into 5-μm-thick sections for histological examination. Toluidine blue staining and Hematoxylin and Eosin (H&E) staining were performed to observe the reconstruction of the injured growth plates. To evaluate the expression of chondrogenesis-related genes in the growth plate defects, immunocytochemical staining of COL II and COL X was carried out. Moreover, the immunocytochemical staining of OCN was also performed to study the severity of bony bar formation.

2.12. Statistical analysis

All data in the study were presented as means ± standard deviations (SDs). The statistical analysis was performed (ANOVA with Tukey's post-hoc analysis) with SPSS 19.0 (SPSS Inc., Chicago, IL, USA). $P < 0.05$ was considered statistically significant. All experiments were repeated at least three times.

3. Results and discussion

3.1. Design and characterization of the 3D-printed bioinspired stratified scaffolds

The growth plate is a cartilage tissue composed of chondrocytes and the extracellular matrix (ECM). It is an avascular and aneural area just like other cartilaginous tissues, its nutrition depends on the vascular system in the adjacent bony tissue [26]. The structure of the growth plate consists of three distinct zones, and each zone contains chondrocytes at different levels of differentiation. From the epiphysis to the diaphysis, the growth plate is divided into the resting zone, the proliferative zone, and the hypertrophic zone [27]. The resting zone is close to the epiphysis and contains chondrocytes that function as progenitor cells, and these cells are going to develop into the volume of chondrocytes in the proliferative zones [28]. In the hypertrophic zone, the chondrocytes mainly produce collagen X (COL X) and undergo cell death [29].

To fabricate an anatomy-inspired bionic scaffold, the tissue structure of the growth plate was investigated in detail. The three regions of the growth plate were distinctly observed in histological sections of four-week-old rabbits. The gradient structure was obvious in the H&E stain (Fig. 1A), the toluidine blue stain (Fig. 1B), and the Masson stain

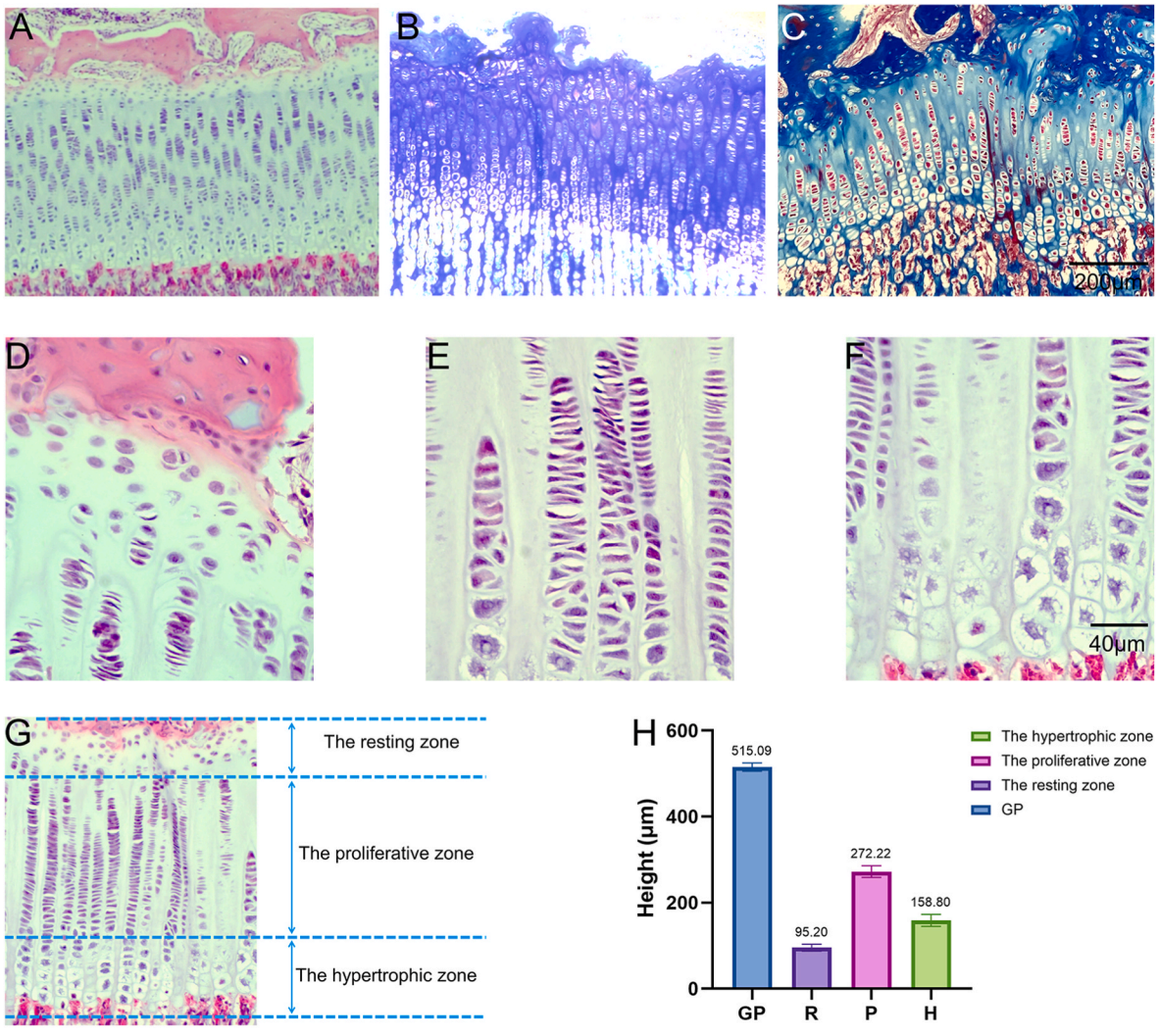

Fig. 1. Structure of the normal growth plate in four-week-old rabbits. (A) H&E staining. (B) Toluidine blue staining. (C) Masson staining of the structure of the growth plate. (D) Resting zone. (E) Proliferative zone. (F) Hypertrophic zone of the growth plate. (G) Distinction of each zone. (H) Calculation of the height in three zones. (For interpretation of the references to colour in this figure legend, the reader is referred to the Web version of this article.)

(Fig. 1C), which indicated that the chondrocytes were in a columnar arrangement in the growth plate. The cartilaginous progenitor cells in the resting zone were small and flat-shaped near the articular surface (Fig. 1D). The chondrocytes in the proliferative zone were arranged in a columnar manner. These cells were homogeneously derived from resting cells (Fig. 1E). Hypertrophic chondrocytes in the hypertrophic zone were the most typical to figure out (Fig. 1F). Hypertrophic chondrocytes were much bigger than chondrocytes in the other two regions. Cells were transparent in the H&E and toluidine blue stains. Through calculations, we found that the total height of the growth plate in four-week-old rabbits was around 500 μm. The height of the resting zone was about 95 μm. The heights of the proliferative zone and hypertrophic zone were approximately 272 μm and 159 μm (Fig. 1G). Therefore, the ratio of the three zones (resting, proliferative, and hypertrophic) was approximately 2:5:3 (Fig. 1H). The 3D-printed biomimetic scaffolds were designed according to the ratio of the three zones. The height ratio in the bionic scaffolds was set as 2:5:3 (small-pore region: medium-pore region: large-pore region).

Bioinspired scaffolds for the implantation of growth plate defects were designed to be 2 mm thick per previous studies [25,30,31]. During 3D printing, the layer height was set as 0.2 mm, and each bionic scaffold had 10 layers. Therefore, there were 2, 5, and 3 layers. From the general Figure of the scaffolds (Fig. 2A), the bottom view and the top view of the scaffolds were different. In the bottom view, it was obvious that the pore size was rather small. In the top view, the large-pore region had more porous structures. The height of the bioinspired stratified scaffolds was 2 mm from the lateral view in Fig. 2A. To observe the three regions distinctly, each region was printed individually in Fig. 2B. The pore sizes in the three regions were visible, especially through light microscopy (Fig. 2C). Changing the printing speed affected the pore sizes, with a higher speed leading to a larger pore size. Moreover, the string sizes were affected as well. With a higher speed, the string was rather thin; whereas, with a lower speed, the string sizes thick. From the lateral view of the scaffold obtained through SEM (Fig. 2D), a distinct three-layer gradient structure is evident. Furthermore, the lateral observation reveals a uniform distribution of struts and a well-organized pore pattern in each layer. Through quantitative analyses, the string sizes in the small-pore region, medium-pore region, and large-pore region were 539.64 ± 16.03 μm, 395.01 ± 6.88 μm, and 261.16 ± 14.56 μm respectively (Fig. 2E). The mean pore sizes in the different regions were 88.05 ± 7.32 μm, 224.35 ± 7.05 μm, and 404.18 ± 26.98 μm (Fig. 2F). It was obvious that the printing process was stable throughout the

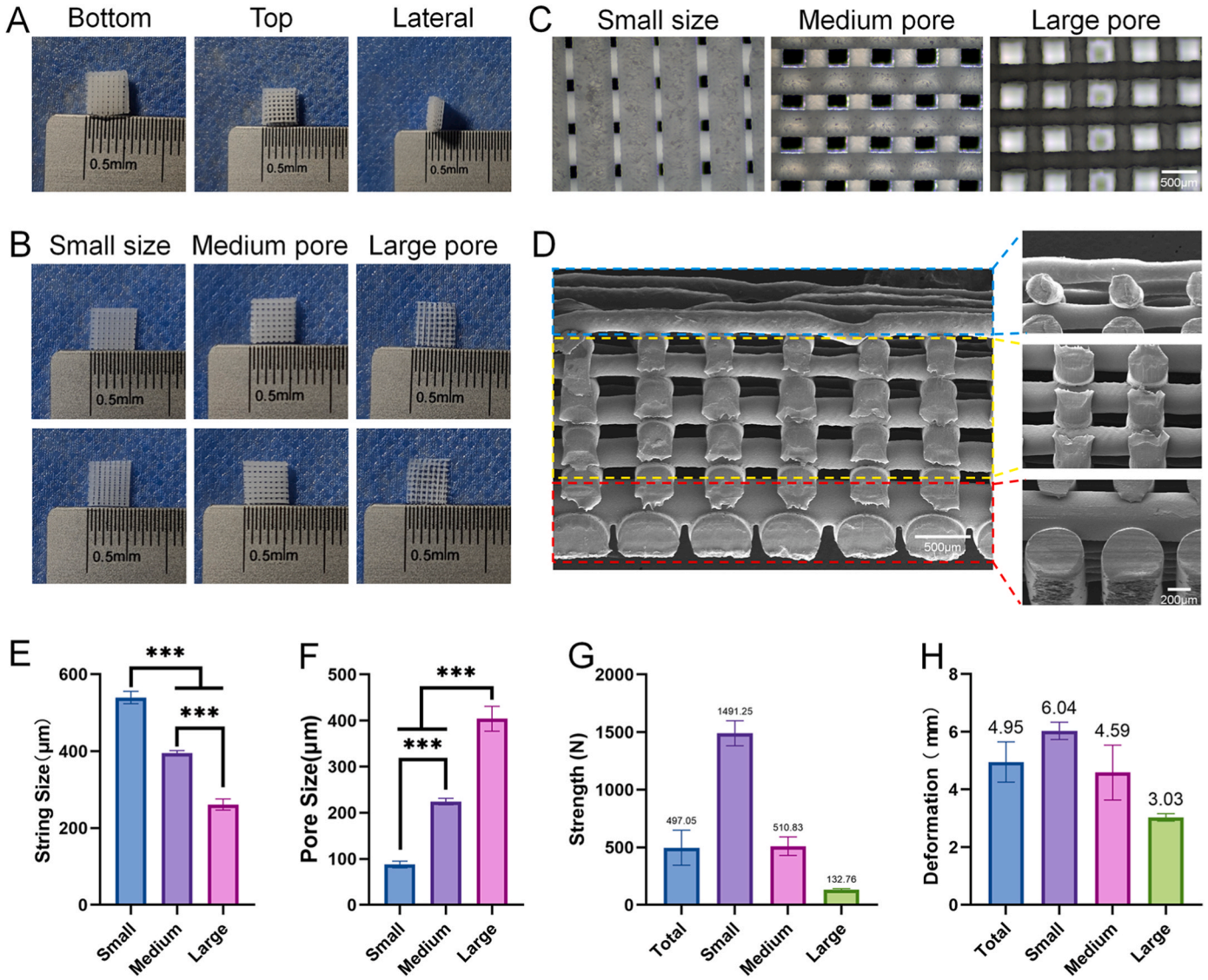

Fig. 2. Characteristics of the 3D-printed stratified scaffolds. (A) Gross image of the 3D-printed stratified scaffold. (B) Gross images of the three regions. (C) Images of the three regions under the light microscope. (D) SEM images of the scaffold in lateral view. (E) String sizes of each region in the scaffold. (F) Pore sizes of each region in the scaffold. (G) Maximum forces of the stratified scaffold for each region. (H) Extension at the maximum force of the stratified scaffold for each region.

procedure. The string size was uniformly distributed in each layer. The pore sizes were similar as predesigned. As for the most suitable pore size in chondrogenesis, Han et al. have reported that scaffolds with pore sizes of 100–200 μm can significantly induce chondrocyte proliferation and chondrogenic-related gene expression. Therefore, it will promote the deposition of the cartilaginous matrix (such as COL II and aggrecan). However, scaffolds with small (<50 μm) or large (>400 μm) pores are unsuitable for chondrocyte-related proliferation and differentiation [32]. Similarly, Han K.-S. et al. also demonstrated that 90–250-μm pores provided the most suitable environments for chondrocyte proliferation. The chondrocyte markers of aggrecan and COL II were highly expressed under these pore sizes as well [33]. As for large-pore-size regions, the pore size will induce the modification of the chondrocyte phenotype if it is unsuitable for chondrocyte proliferation [34]. In summary, the 90–250-μm pore size may induce BMSCs to proliferate and become chondrocytes, the same as chondrocytes in the proliferative zone of the growth plate. Meanwhile, large pores (>400 μm) may transform chondrocytes into hypertrophic chondrocytes, just like those in the hypertrophic zone [35,36]. Therefore, it is rational for the bionic stratified scaffold to stimulate BMSCs to differentiate into structures similar to those in the growth plate as previous studies reported.

Since the scaffolds were going to be implanted in the bones, it was important for them to have some load-bearing capacity and compression-resistance ability. Upon testing the mechanical properties of the stratified scaffolds (Fig. 2G and H, and S1), the results showed that the stratified scaffolds were able to bear some weight. The maximum strength was approximately 500 N. The mechanical properties were different for all stratified scaffolds and the three regions. The small-pore region showed the maximum strength compared with the other regions. The strength of the stratified scaffolds was between the medium-pore region and the large-pore region. In summary, the stratified scaffolds were successfully 3D printed. It had three distinct regions with different pore sizes as predesigned. The stratified scaffolds were demonstrated to be strong enough for-load bearing in children.

3.2. Surface modification

As a hydrophobic biological biomaterial, PCL was not suitable for cell adhesion [37]. To promote cell viability on the surfaces of scaffolds, we compared three effective surface modification strategies. These modifications were poly-D-lysine coating, NaOH corroding, and COL I coating after NaOH corrosion. For cell experiments, as shown in Fig. 3A, the live/dead staining demonstrated that all these strategies were biocompatible (Fig. 3B). BMSCs were in good condition on the scaffolds.

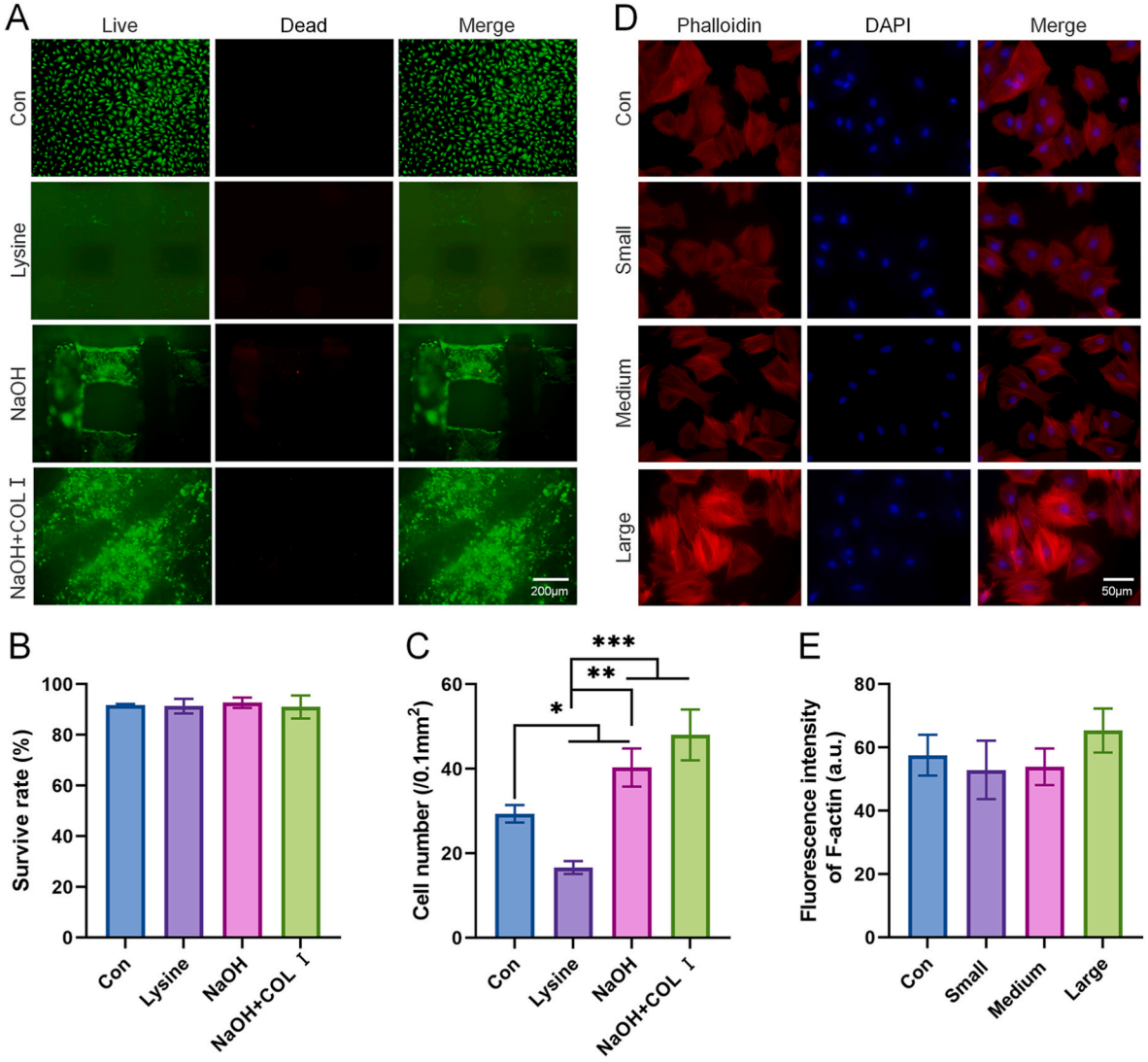

Fig. 3. Biocompatibility of 3D-printed scaffolds with or without surface modification. (A) Live/dead staining of different surface modification strategies. (B) Quantitative analysis of BMSC viability. (C) Quantitative analysis of the BMSC densities of different groups. (D) Rhodamine-phalloidin staining of the modified scaffolds. (E) Quantitative analysis of the F-actin fluorescence in BMSCs. (*$p < 0.05$, **$p < 0.01$, ***$p < 0.001$).

The results showed that the modification of COL I coating after NaOH corrosion resulted in the most cell adhesion (Fig. 3C). Meanwhile, the poly-D-lysine coating resulted in much less cell adhesion, and NaOH corrosion had an effect that was midway between those of the other two strategies. This result indicated that COL I coating after corrosion benefited BMSCs by enabling them to attach to the PCL scaffolds.

Because the modification of COL I coating after NaOH corrosion had the best effect on cell adhesion, in subsequent experiments, this strategy was applied throughout. Cell morphologies of the modified scaffolds were also tested by rhodamine-phalloidin staining. As shown in Fig. 3D, the F-actin filaments of BMSCs were well-organized in modified scaffolds in each region compared to the control group. The morphologies of BMSCs were well-formed, and no adverse effects were observed (Fig. 3E). Since the F-actin filaments are critical for cell adhesion, proliferation, and differentiation, the modified scaffolds were beneficial to the cell function of BMSCs. It is effective to use NaOH and COL I for surface modification to enhance cell adhesion to the PCL scaffolds.

In the modified three-layer scaffold structure, cells within the small and medium pore region appeared to exhibit relatively smaller sizes, while those within the large pore region seemed to adopt larger and more spread-out morphologies. This observation suggests that the expansive environment of the large pore region potentially facilitates easier nutrient access, leading to the observed differences in cell size and spreading patterns.

Many previous studies have proven that NaOH corrosion is an effective strategy because it can improve the PCL surface roughness and cytocompatibility [38,39]. In a comparative study, Zamani et al. compared the effect of NaOH to RGD-induced modifications. Different concentrations (1 M, 3 M, and 5 M) were tested for 24 h and 72 h. According to the results, a 24-h 3 M NaOH treatment could enhance cell adhesion and matrix deposition just as well as RDG immobilization. More importantly, a 24-h NaOH treatment could also promote the formation of osteogenic cells while RGD immobilization could not [17]. Therefore, 24-h 3 M NaOH treatment is an effective strategy for PCL surface modification as previously reported.

To figure out the potential mechanism of surface modification, SEM and water contact angle measurements were carried out. As shown in Fig. 4A, SEM images showed that the primary scaffolds had a rather smooth surface. The NaOH modification changed the surface topography of the scaffolds from a smooth to a rough surface pattern. Moreover, the COL I coating made the surface much more uneven. COL I acted as a rope entangled on the surfaces of the scaffolds. It also looked like a web inside the pores. Therefore, the rope on the surface would make it easier for cells to climb and adhere, and the web would provide more space for cell adhesion, migration, and communication. It is well-known that hydrophilicity is associated with cell adhesion [40]. The modification of PCL scaffolds may change the hydrophilicity of the surface. The result of the water contact angle measurement in Fig. 4B and S2 revealed that the surface of the primitive PCL was hydrophobic, and its water contact angle was $104 \pm 3.70^{\circ}$. The modification brought about by the NaOH and COL I treatments significantly changed the hydrophilicity of the surface, as evidenced by water contact angles of $78.29 \pm 4.59^{\circ}$ and $56.09 \pm 1.72^{\circ}$, respectively (the water contact angles were significantly reduced after the modification). The hydrophobicity of the initial PCL surface was due to the hydrophobic nature of PCL biomaterials [41]. After corrosion by the 3 M NaOH solution and COL I coating, the smooth surfaces of PCL scaffolds became rougher. Therefore, the modified surface enhanced the hydrophilicity of PCL scaffolds. Moreover, because of its excellent water absorption property, the presence of COL I would further improve the hydrophilicity of the scaffold's surface. It is well-known that high hydrophilicity is beneficial to cell adhesion [42].

Traditional modification methods for PCL materials include RGD surface modification [43], platelet-rich plasma coating [44], Polydopamine coating [45]. However, these methods often involve expensive reagents and complex procedures, making it challenging to translate them to clinical applications [46]. In this study, we evaluated several modification approaches and ultimately selected a surface modification method involving a 24-h treatment with 3 M NaOH solution followed by COL I coating. This chosen modification approach is simple to perform, the materials are readily available, and it is cost-effective. After modification, the results demonstrated a significant increase in cell adhesion efficiency. Moreover, the mechanism of this modification approach is straightforward: it mainly alters the scaffold surface roughness and hydrophilicity, thereby enhancing cell adhesion efficiency, as confirmed by scanning electron microscopy and water contact angle tests. The simplicity and effectiveness of this modification approach make it a promising candidate for further studies and potential clinical applications.

3.3. The most suitable co-culture ratio for chondrogenesis

It was necessary to incorporate stem cells to promote local chondrogenesis to reconstruct the injured growth plate since a bare scaffold was insufficient. BMSCs were the most frequently used pluripotent stem cells in bone and cartilage repair. However, BMSCs alone were not sufficient, and chondrogenic growth factors, including insulin-like growth factor-1 (IGF-1), fibroblast growth factor-2 (FGF-2), and transforming growth factor-β1 (TGF-β1) were also used in previous studies to induce BMSC differentiation [47]. In this study, we used the co-culture of chondrocytes and BMSCs to achieve the reconstruction of the injured growth plate. To find the most suitable ratio of two cells for chondrogenesis, the CCK-8 experiment was performed. As shown in Fig. 4C, the relative cell proliferation speeds were rather different among different ratios of two cells on the 3D-printed modified scaffolds. On day 4, the co-culture group of chondrocytes and BMSCs in 1:1, 1:2, and 1:3 ratios showed better results than the other groups. On day 7, the 1:1 and 1:3 co-culture groups showed the best results as the relative cell proliferation rates were higher in these two groups than in the other five groups; however, the difference between them was not statistically significant. The most suitable ratio will be selected by chondrogenic differentiation-related experiments. To do this, the chondrogenesis-related proteins, COL II and GAG, were tested by ELISA. As shown in Figs. S3 and 4D, the 1:3 ratio in the co-culture group showed a higher protein concentration than the ratio in any of the other groups. Similarly, Alcian blue staining also showed the highest intensity under this co-culture ratio among all the groups as shown in Fig. 4E and S4. In summary, the co-culture ratio of chondrocytes and BMSCs showed the best results for cell proliferation in the 1:1 and 1:3 ratios. However, when it comes to chondrogenic differentiation, the 1:3 group showed the best results. Therefore, we confirmed that the 1:3 co-culture ratio was most suitable for chondrogenesis. In the following experiments, the co-culture of these two cells was performed in this ratio.

In previous studies, it has been demonstrated that the co-culture of chondrocytes and BMSCs will improve the proliferation ability and cartilage phenotype [48]. It is believed that the most promising cell application of cartilaginous tissue engineering is the co-culture of chondrocytes and MSCs. Because the existence of chondrocytes will induce stem cell differentiation, and the presence of stem cells will also promote cell proliferation. The co-culture will solve the problems of chondrocyte obtention and expansion [49]. As for the most suitable ratio, it is still controversial. Many studies have used the 1:1 and 1:3 ratios. In a detailed study, Kim et al. tested the co-culture of chondrocytes and synovium-derived mesenchymal stem cells in different ratios. The group with the 1:3 ratio demonstrated the largest GAG content and the highest GAG/DNA ratio. However, COL II and Sox-9 were upregulated in the 1:1 ratio compared to the 1:3 ratio [50]. The BMSCs are different from synovium-derived mesenchymal stem cells. It is important to test the co-culture of chondrocytes and BMSCs. In another study, Qing et al. evaluated the chondrogenesis of articular chondrocytes and BMSCs co-culture, and they concluded that the optimal co-culture ratio was 2:1 [51]. However, they only tested the 4:1, 2:1, 1:1, 1:2, and 1:4 ratios and did not test the 1:3 ratio. Considering the

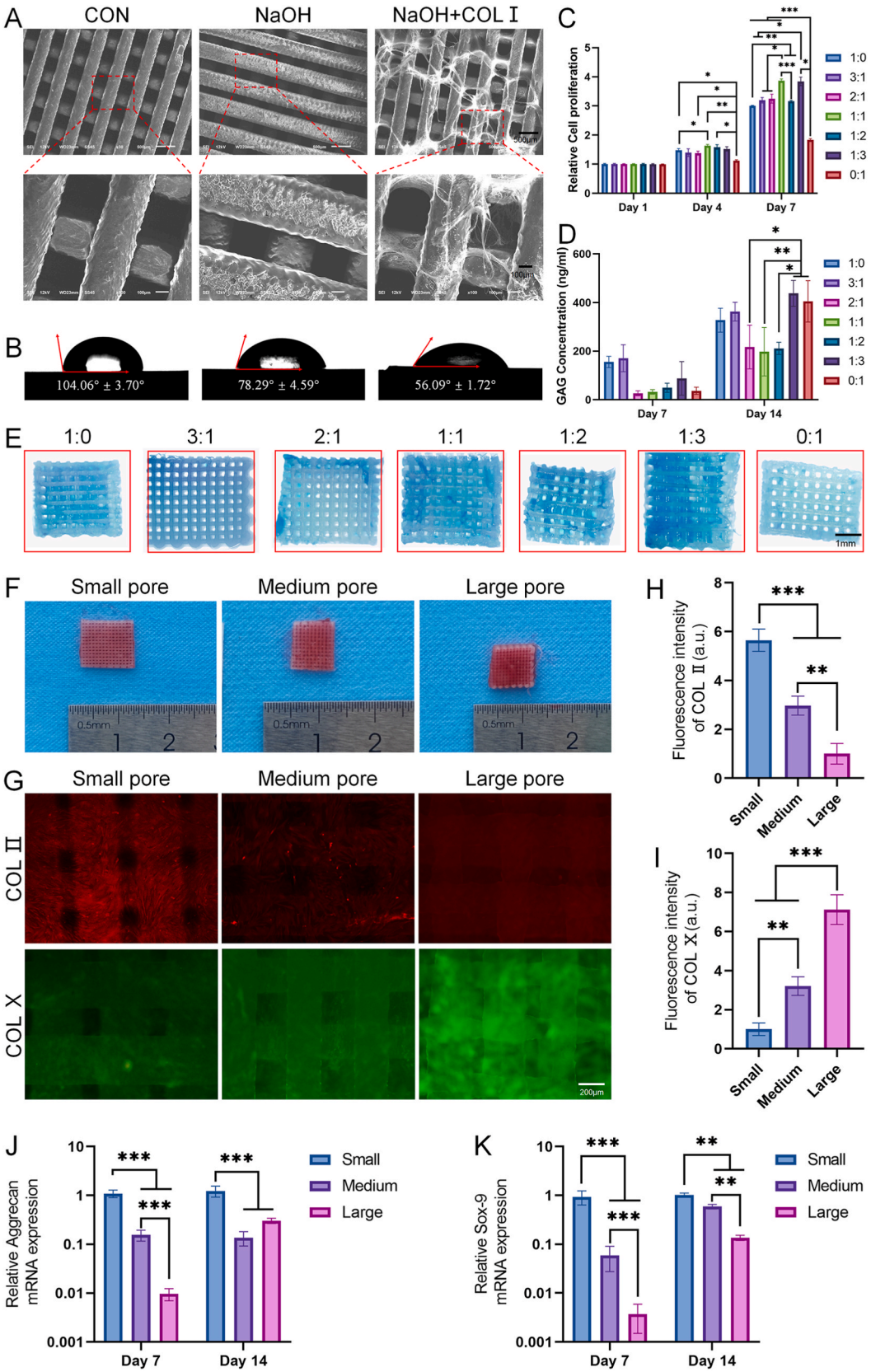

Fig. 4. Surface modification and the most suitable co-culture ratio for chondrogenesis. (A) SEM images of the scaffold after different modifications. (B) Images of the water contact angle test. (C) CCK-8 results of the co-culture of chondrocytes and BMSCs in different ratios. (D) ELISA results of GAG in the co-culture of chondrocytes and BMSCs in different ratios. (E) Alcian blue staining in different ratios. (F) Safranin O and Fast Green staining on the three regions of the scaffold. (G) Immunofluorescence staining of cartilage-related proteins. (H) Quantitative statistics COL II expression. (I) Quantitative statistics COL X expression. (J) Quantitative analysis of the chondrogenic gene of Aggrecan. (K) Quantitative analysis of the chondrogenic gene, *Sox-9*. (*p < 0.05, **p < 0.01, ***p < 0.001). (For interpretation of the references to colour in this figure legend, the reader is referred to the Web version of this article.)

specific environments of 3D-printed stratified scaffold surfaces in our study, things may differ. Involving all the results we got and previous research conclusions, we believe the 1:3 (chondrocytes to BMSCs) co-culture ratio is the optimal selection for growth plate reconstruction.

3.4. The induction of chondrogenesis in the three regions of scaffolds

The pore size influences chondrogenesis [52]. To investigate the chondrogenic differentiation in three regions, cartilage-related proteins staining and RT-qPCR experiments were performed. By performing Safranin O and Fast Green staining on the three regions of the scaffold, as depicted in Fig. 4F, all three regions exhibited positive Safranin O staining and negative Fast Green staining. From the Safranin O staining, it is evident that the large pore region displayed the deepest coloration, followed by the medium pore region, while the small pore zone exhibited the lightest coloration. Deeper staining indicates higher secretion of cartilaginous matrix. These results suggest that the large pore region resembles the hypertrophic zone of the growth plate, with chondrocytes maturing and actively synthesizing abundant extracellular matrix. Conversely, the medium and small pore zones share similarities with the proliferation and resting zones, with lower extracellular matrix secretion and cells maintaining certain proliferative characteristics.

In Fig. 4G and H, it can be seen that the COL II protein was more highly produced in the small-pore region than in the other two regions. In the medium- and large-pore regions, the COL II protein was much less produced, especially in the large-pore region. As for the immunofluorescence of COL X, it is obvious that the latter was mainly produced in the large-pore region, with a little in the medium- and small-pore regions as shown in Fig. 4G and I. It is well known that COL II is associated with chondrocyte proliferation and cartilage phenotype maintenance [53]. Therefore, the small- and medium-pore regions were beneficial to chondrocyte proliferation and retain their differentiation capacity. This was similar to what happened in the resting and proliferative zones. Moreover, the expression of cartilage-related genes, *Aggrecan* and *Sox-9*, were also evaluated. As shown in Fig. 4J and K, the cartilage-related genes were highly expressed in the small- and medium-pore regions.

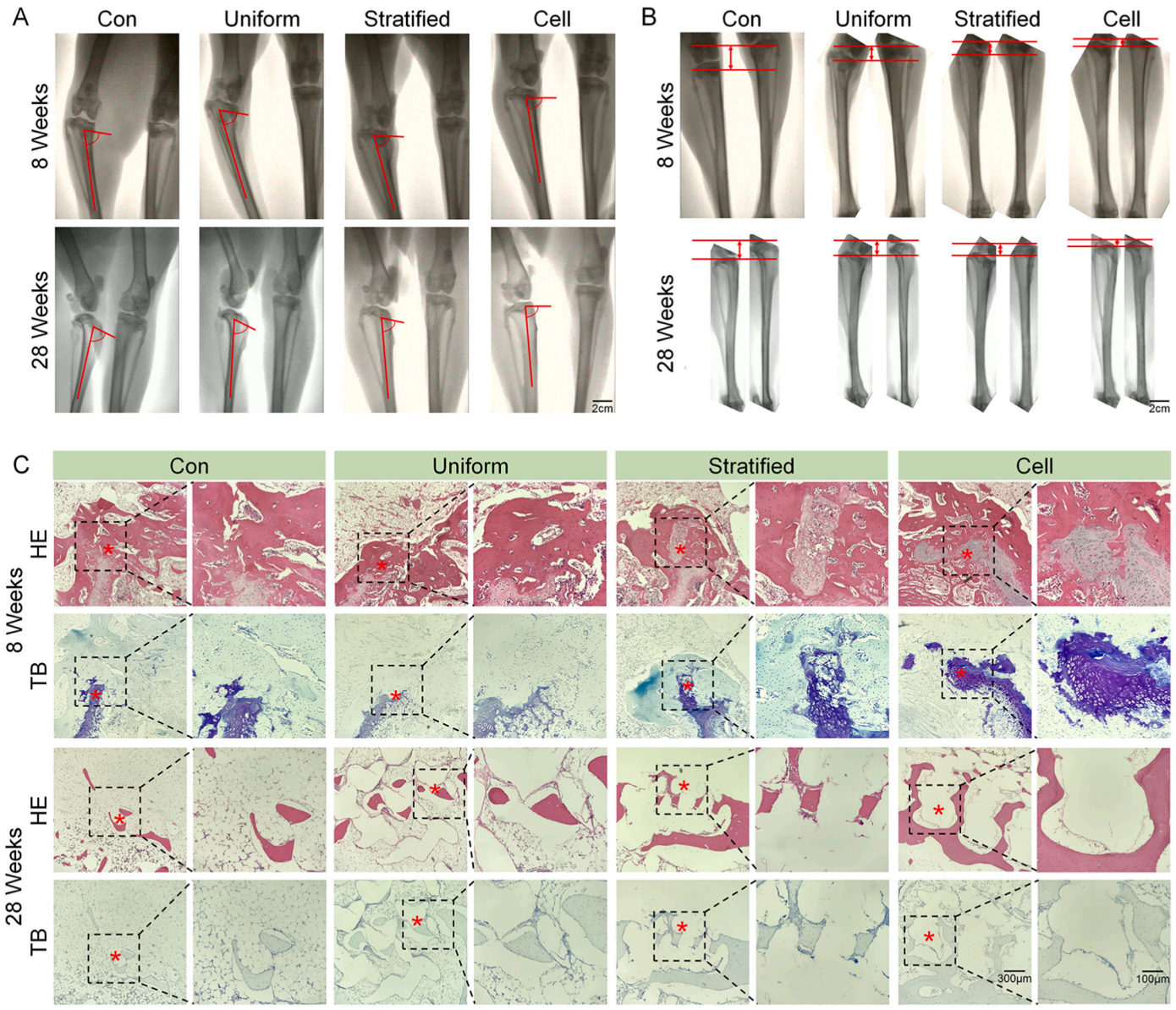

Fig. 5. (A) X-ray image of the angular deformities of the tibia. (B) X-ray image of the length discrepancy of the tibia. (C) H&E and toluidine blue staining of the reconstructed growth plate at 8 weeks and 28 weeks (The asterisks in the figure denote the location of the growth plate defect region). (For interpretation of the references to colour in this figure legend, the reader is referred to the Web version of this article.)

The large-pore region showed the lowest expression level of all regions. Many studies have explored the association between pore size and chondrocyte behavior [54]. It has been agreed upon that small pores (90–250 μm) will significantly promote chondrocyte proliferation and chondrogenic gene expression [32]. Meanwhile, large pores (>400 μm) will induce chondrocyte hypertrophy and apoptosis [19]. The mechanisms involved are still unclear. In a previous study, Di Luca et al. found that the oxygen tension and nutrient availability changed with the different pore sizes. With large pores, nutrients were abundant and the oxygen tension was high. However, with small pores, the oxygen tension and nutrient availability were decreased [22]. It is confirmed that the low oxygen level will promote chondrocyte proliferation and abundant nutrient supplies will promote chondrocyte senescence [55]. Therefore, the effects of pore sizes on chondrocyte behavior might be related to oxygen tension and nutrient availability.

3.5. Reconstruction of the growth plate in vivo

3.5.1. Evaluation of the tibial length and tibial angle

The details of the growth plate defect animal model are shown in Fig. S5. After preparing the growth plate defect, the most severe consequences of growth plate injury are limb length discrepancy and angular deformity [56]. Radiography was performed on the animals to evaluate the function of the regenerated growth plate. As shown in Fig. 5A and B, the angular deformity and limb length discrepancy in each group were rather different. To measure the tibial lengths and angles, the standardized measurement method was applied as previously described (Fig. S6) [25]. The tibial length was measured along the bone's long axis, from the tibiotalar joint line to the tibial plateau line. The angle measured was the one between the tibial plateau line and the long axis line of the tibia. At eight weeks, the deformity angles were much lower in the control and uniform-pore-size groups, and there was no significant difference in this parameter between them. The stratified scaffolds group and the cell-loaded group had milder angular deformity than the other two groups since their deformity angles were close to 90° (normal condition). At 28 weeks, the growth plate disappeared and was replaced by the linear epiphysialis. At this point, the results of long-term effects were revealed. The cell-loaded group had the mildest angular deformity. Then, the stratified scaffold group had milder angular deformity than the control and uniform-pore-size groups. At 28 weeks, the uniform-pore-size group showed milder angular deformity than the control group. The uniform-pore-size scaffolds also had repair effects (Fig. S7). The limb length discrepancy results are shown in Fig. S8. At 8 weeks, the limb length discrepancy was much smaller in the stratified and cell-loaded groups than in the other two groups; however, there was no significant difference in this parameter between them. At 28 weeks, the limb length discrepancy was lowest in the cell-loaded group, followed by the stratified group and the uniform group, while the control group had the highest limb length discrepancy. The results of the tibial length and tibial angle showed that even the uniform scaffolds had some repair effect. The stratified scaffolds would do better and maybe contribute to the layered effects of inducing chondrogenesis. The 3D-printed scaffolds with a gradient pore size structure seemed to be a promising method of promoting a hierarchical chondrogenic differentiation of local chondrocytes. Moreover, the cell-loaded groups showed better results than the stratified groups, perhaps due to the presence of chondrocytes and BMSCs. In growth plate defects, the number of chondrocytes was limited. Stratified scaffolds alone were not enough. The supplemental chondrocytes would proliferate and produce cartilaginous ECM to fill the defects. Therefore, the 3D-printed stratified scaffolds loaded with chondrocytes and BMSCs will be more effective for growth plate reconstruction.

3.5.2. Chondrogenesis and reconstruction of the injured growth plate tissue

To find investigate growth plate reconstruction at the tissue level, H&E and toluidine blue staining were performed. As shown in Fig. 5C, at 8 weeks, H&E staining revealed that there was bony bar formation in the control group. The growth plate injury was successfully established. From the image of the control group in H&E and toluidine blue staining, only a few cartilaginous-like tissues were observed. Chondrocytes were distributed in a disorderly manner. In the uniform-pore-size group, the scaffolds provided support for the defect area. More chondrocytes were observed in the defects; however, these cells were randomly distributed as well. Unlike in the control and uniform groups, in the stratified group, more cartilaginous-like tissues were observed in the defects. Chondrocytes were placed in a certain distribution pattern, which may have been induced by the stratified structure of the scaffolds. More importantly, the cell-loaded group showed the largest amount of cartilaginous tissue. Chondrocytes in the growth plate defects were well-distributed, and neogenetic tissues had a similar structure to that of the normal growth plate. At 28 weeks, the growth plate disappeared and was replaced by the linea epiphysialis. Tissue section staining demonstrated that only a few bone trabeculae emerged in the control group. The linea epiphysialis was incomplete. Although more bone trabeculae appeared in the uniform group, they were scattered and the linea epiphysialis was incomplete as well. The stratified and cell-loaded groups showed a continuous linea epiphysialis. More bone trabeculae were observed in the defects, which means growth plate reconstruction was similar to a physiological process.

Furthermore, immunocytochemical staining of cartilage- and bone-related proteins was also evaluated. As shown in Fig. 6A and B, at 8 weeks, the osteogenesis-related protein, OCN, was highly produced in the control and uniform groups. The OCN was at a low level in the other two groups. On the contrary, the chondrogenesis-related proteins, COL II and COL X, were at a low level in the control and uniform groups. At 8 weeks, the COL II protein was highly expressed in the stratified and cell-loaded groups as shown in Fig. 6A. COL X was also expressed at a higher level than in the control and uniform groups; however, its expression was not as high as that of COL II (Fig. 6A and C). No significant difference was observed between the stratified group and the cell-loaded group (Fig. 6A and D). At 28 weeks, because the growth plate was replaced by the linea epiphysialis, immunocytochemical staining of COL II and COL X revealed no positive results. However, from immunocytochemical staining of OCN in Fig. 6E and F, the cell-loaded group presented the highest level of bone formation at 28 weeks. The stratified group also showed a higher level of OCN than the other two groups. In conclusion, all these results indicated that the use of cell-loaded stratified scaffolds is the most suitable approach for growth plate reconstruction. In the early phase (within eight weeks), the cell-loaded scaffolds will provide support for the defects. The cells on the scaffolds will proliferate and differentiate as induced by the stratified structure. These efforts will rebuild the columnar structure of the growth plate. In the long run, the growth plate will undergo a process similar to that undergone by the normal growth plate in the cell-loaded group.

4. Conclusion

In this study, we prepared a bioinspired bionic PCL scaffold with chondrocyte and BMSC loading for the treatment of growth plate injuries. The bioinspired stratified scaffolds had three distinct regions with different pore sizes; i.e., small, medium, and large. The height of each region was designed to be the same as the three zones in the growth plate. The scaffolds were modified by NaOH treatment and COL I coating to improve cell adhesion. *In vitro* experiments demonstrated that the optimal ratio for the chondrogenesis of the co-culture of chondrocytes and BMSCs was 1:3 on the stratified scaffold. It was also proven that the stratified scaffold was able to induce chondrocytes to become organized, the same as the chondrocytes in the growth plate. After being implanted in growth plate defects, cell-loaded stratified scaffolds successfully reconstructed the growth plate. The injured growth plate went through a biological process similar to that undergone by the normal growth plate. Therefore, the use of this kind of chondrocyte and BMSC-loaded

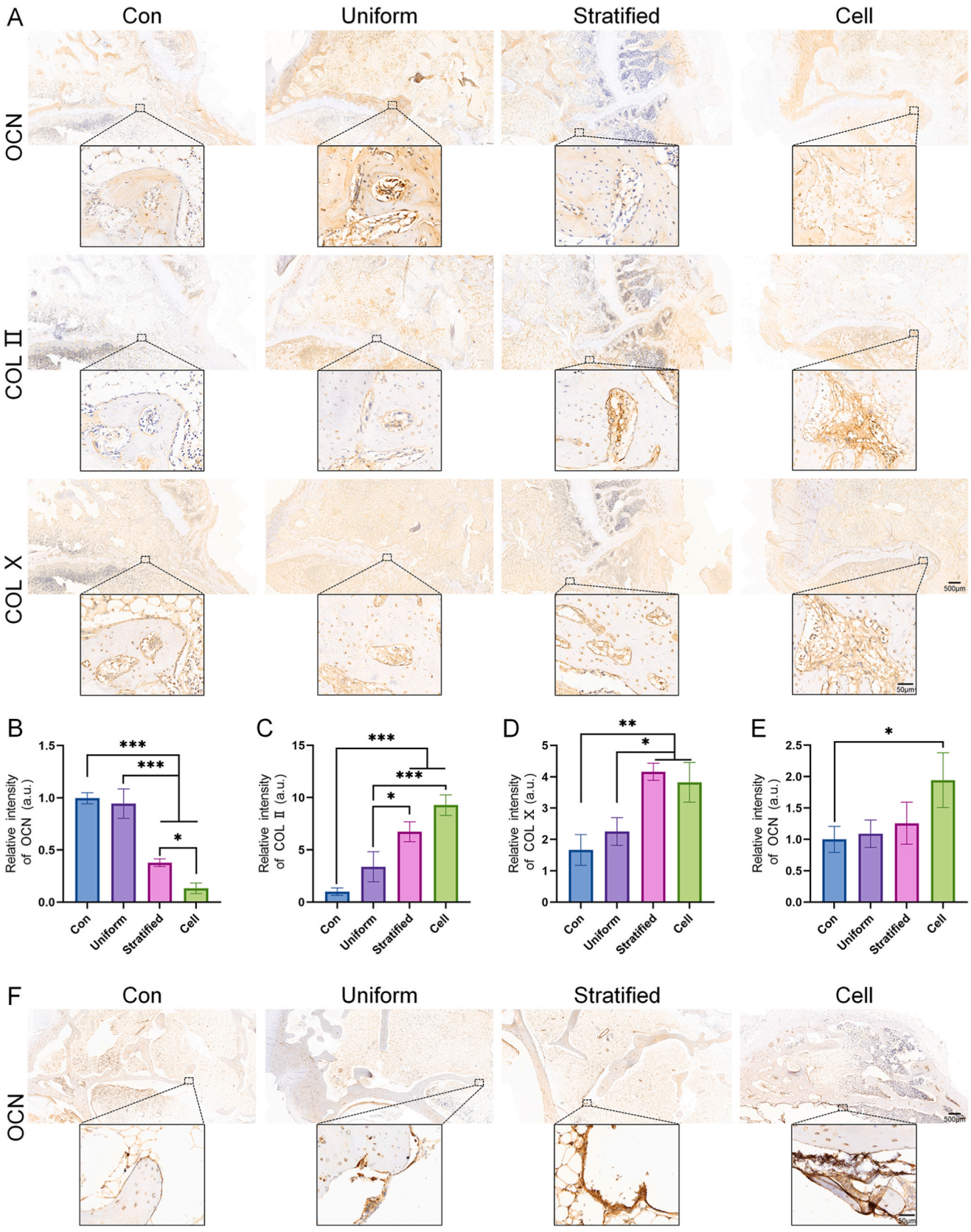

Fig. 6. Immunocytochemical staining of the reconstructed growth plate. (A) Immunocytochemical staining of different proteins at the reconstructed growth plate at 8 weeks. Quantitative analyses of the (B) OCN protein, (C) COL II protein, and (D) COL X protein at 8 weeks. (E) Quantitative analysis of the OCN protein at 28 weeks. (F) Immunocytochemical staining of OCN proteins at the reconstructed growth plate at 28 weeks. (*$p < 0.05$, **$p < 0.01$, ***$p < 0.001$).

stratified scaffold was confirmed to be a promising approach for growth plate reconstruction.

Credit author statement

Xianggang Wang: Conceptualization, Methodology, Investigation, Data curation, Formal analysis, Write-Original draft. **Zuhao Li:** Methodology, Formal analysis, Software. **Jiaqi Liu:** Methodology, Formal analysis. **Chenyu Wang:** Methodology, Investigation. **Haotian Bai:** Methodology, Investigation. **Xiujie Zhu:** Methodology, Investigation. **Hui Wang:** Validation, Investigation. **Zhonghan Wang:** Validation, Investigation. **He Liu:** Conceptualization, Writing - Review & Editing, Project administration, Funding acquisition. **Jincheng Wang:** Writing - Review & Editing, Supervision, Validation, Project administration, Funding acquisition.

CRediT authorship contribution statement

Xianggang Wang: Conceptualization, Methodology, Investigation, Data curation, Formal analysis, Writing – original draft. **Zuhao Li:** Methodology, Formal analysis, Software. **Jiaqi Liu:** Methodology, Formal analysis. **Chenyu Wang:** Methodology, Investigation. **Haotian Bai:** Methodology, Investigation. **Xiujie Zhu:** Methodology, Investigation. **Hui Wang:** Validation, Investigation. **Zhonghan Wang:** Validation, Investigation. **He Liu:** Conceptualization, Writing – review & editing, Project administration, Funding acquisition. **Jincheng Wang:** Writing – review & editing, Supervision, Validation, Project administration, Funding acquisition.

Declaration of competing interest

The authors declare no conflict of interest related to this article.

Data availability

Data will be made available on request.

Acknowledgments

This work was supported by the National Natural Science Foundation of China (Grant Nos. 82001971, 82102358, and 82202698), the Scientific Development Program of Jilin Province (Grant Nos. 20200403088SF, 20220204117YY, YDZJ202201ZYTS086, 20200404202YY, and 20200802008 GH); the Program of Jilin Provincial Health Department (Grant No. 2020SC2T064 and 2020SC2T065), the Project of the "Medical + X" Interdisciplinary Innovation Team of Norman Bethune Health Science Center of Jilin University (Grant No. 2022JBGS06), the China Postdoctoral Science Foundation (Grant No. 2021M701384), and the Bethune Plan of Jilin University (Grant No. 2022B27).

Appendix A. Supplementary data

Supplementary data to this article can be found online at https://doi.org/10.1016/j.mtbio.2023.100833.

References

[1] Y. Miyazaki, A. Ichimura, R. Kitayama, N. Okamoto, T. Yasue, F. Liu, T. Kawabe, H. Nagatomo, Y. Ueda, I. Yamauchi, T. Hakata, K. Nakao, S. Kakizawa, M. Nishi, Y. Mori, H. Akiyama, K. Nakao, H. Takeshima, C-type natriuretic peptide facilitates autonomic Ca(2+) entry in growth plate chondrocytes for stimulating bone growth, Elife 11 (2022), e71931.

[2] M. Shen, S. Liu, X. Jin, H. Mao, F. Zhu, T. Saif, R. Zhou, H. Fan, P.C. Begeman, C. C. Chou, K.H. Yang, Porcine growth plate experimental study and estimation of human pediatric growth plate properties, J. Mech. Behav. Biomed. Mater. 101 (2020), 103446.

[3] A.A. Czitrom, R.B. Salter, R.B. Willis, Fractures involving the distal epiphyseal plate of the femur, Int. Orthop. 4 (4) (1981) 269–277.

[4] R.B. Salter, Injuries of the epiphyseal plate, Instr. Course Lect. 41 (1992) 351–359.

[5] S. Wang, S. Zheng, Q. Liu, C. Wang, M. Liu, L. Su, Value of growth arrest lines for predicting treatment effect on children with distal tibial epiphysis fractures, Front. Pediatr. 11 (2023), 1040801.

[6] L. Lin, S. Jiang, J. Yang, J. Qiu, X. Jiao, X. Yue, X. Ke, G. Yang, L. Zhang, Application of 3D-bioprinted nanocellulose and cellulose derivative-based bio-inks in bone and cartilage tissue engineering, Int. J. Bioprint 9 (1) (2023) 637.

[7] A.S. Tiffany, B.A.C. Harley, Growing pains: the need for engineered platforms to study growth plate biology, Adv. Healthc. Mater. 11 (19) (2022), e2200471.

[8] Y. Zhang, X. Liu, L. Zeng, J. Zhang, J. Zuo, J. Zou, J. Ding, X. Chen, Polymer fiber scaffolds for bone and cartilage tissue engineering, Adv. Funct. Mater. 29 (36) (2019), 1903279.

[9] F. Valipour, F. Valioglu, R. Rahbarghazi, A.M. Navali, M.R. Rashidi, S. Davaran, Thermosensitive and biodegradable PCL-based hydrogels: potential scaffolds for cartilage tissue engineering, J. Biomater. Sci. Polym. Ed. (2023) 1–20.

[10] B. Basturkmen, E. Ergene, D. Doganay, P. Yilgor Huri, H.E. Unalan, E.A. Aksoy, Silver nanowire loaded poly(epsilon-caprolactone) nanocomposite fibers as electroactive scaffolds for skeletal muscle regeneration, Biomater. Adv. 134 (2022), 112567.

[11] E.O. Bachtiar, V.C. Ritter, K. Gall, Structure-property relationships in 3D-printed poly(l-lactide-co-epsilon-caprolactone) degradable polymer, J. Mech. Behav. Biomed. Mater. 121 (2021), 104650.

[12] P. Li, L. Fu, Z. Liao, Y. Peng, C. Ning, C. Gao, D. Zhang, X. Sui, Y. Lin, S. Liu, C. Hao, Q. Guo, Chitosan hydrogel/3D-printed poly(epsilon-caprolactone) hybrid scaffold containing synovial mesenchymal stem cells for cartilage regeneration based on tetrahedral framework nucleic acid recruitment, Biomaterials 278 (2021), 121131.

[13] X. Li, H.M. Yin, K. Su, G.S. Zheng, C.Y. Mao, W. Liu, P. Wang, Z. Zhang, J.Z. Xu, Z. M. Li, G.Q. Liao, Polydopamine-assisted anchor of chitosan onto porous composite scaffolds for accelerating bone regeneration, ACS Biomater. Sci. Eng. 5 (6) (2019) 2998–3006.

[14] C. Yu, M. Xing, S. Sun, G. Guan, L. Wang, In vitro evaluation of vascular endothelial cell behaviors on biomimetic vascular basement membranes, Colloids Surf. B Biointerfaces 182 (2019), 110381.

[15] H.J. Kim, S.J. You, D.H. Yang, J. Eun, H.K. Park, M.S. Kim, H.J. Chun, Injectable hydrogels based on MPEG-PCL-RGD and BMSCs for bone tissue engineering, Biomater. Sci. 8 (15) (2020) 4334–4345.

[16] R. Ghobeira, C. Philips, L. Liefooghe, M. Verdonck, M. Asadian, P. Cools, H. Declercq, W.H. De Vos, N. De Geyter, R. Morent, Synergetic effect of electrospun PCL fiber size, orientation and plasma-modified surface chemistry on stem cell behavior, Appl. Surf. Sci. 485 (2019) 204–221.

[17] Y. Zamani, J. Mohammadi, G. Amoabediny, D.O. Visscher, M.N. Helder, B. Zandieh-Doulabi, J. Klein-Nulend, Enhanced osteogenic activity by MC3T3-E1 pre-osteoblasts on chemically surface-modified poly(epsilon-caprolactone) 3D-printed scaffolds compared to RGD immobilized scaffolds, Biomed. Mater. 14 (1) (2018), 015008.

[18] K. Abbasi, S. Tavakolizadeh, A. Hadi, M. Hosseini, R.S. Soufdoost, A. Heboyan, M. Alam, S. Fani-Hanifeh, The wound healing effect of collagen/adipose-derived stem cells (ADSCs) hydrogel: in vivo study, Vet. Med. Sci. 9 (1) (2023) 282–289.

[19] Z. Abpeikar, P.B. Milan, L. Moradi, M. Anjomshoa, S. Asadpour, Influence of pore sizes in 3D-scaffolds on mechanical properties of scaffolds and survival, distribution, and proliferation of human chondrocytes, Mech. Adv. Mater. Struct. 29 (26) (2021) 4911–4922.

[20] Y. Sun, Y. You, W. Jiang, B. Wang, Q. Wu, K. Dai, 3D bioprinting dual-factor releasing and gradient-structured constructs ready to implant for anisotropic cartilage regeneration, Sci. Adv. 6 (37) (2020), eaay1422.

[21] E. Tamjid, S. Marzooghi, P. Najafi, M. Behmanesh, Three-dimensional gradient porous polymeric composites for osteochondral regeneration, J. Polym. Res. 29 (5) (2022) 163.

[22] A. Di Luca, K. Szlazak, I. Lorenzo-Moldero, C.A. Ghebes, A. Lepedda, W. Swieszkowski, C. Van Blitterswijk, L. Moroni, Influencing chondrogenic differentiation of human mesenchymal stromal cells in scaffolds displaying a structural gradient in pore size, Acta Biomater. 36 (2016) 210–219.

[23] Z. Qiao, M. Lian, Y. Han, B. Sun, X. Zhang, W. Jiang, H. Li, Y. Hao, K. Dai, Bioinspired stratified electrowritten fiber-reinforced hydrogel constructs with layer-specific induction capacity for functional osteochondral regeneration, Biomaterials 266 (2021), 120385.

[24] H. Bai, Y. Zhao, C. Wang, Z. Wang, J. Wang, H. Liu, Y. Feng, Q. Lin, Z. Li, H. Liu, Enhanced osseointegration of three-dimensional supramolecular bioactive interface through osteoporotic microenvironment regulation, Theranostics 10 (11) (2020) 4779–4794.

[25] Y. Yu, F. Rodriguez-Fontan, K. Eckstein, A. Muralidharan, A.C. Uzcategui, J. R. Fuchs, S. Weatherford, C.B. Erickson, S.J. Bryant, V.L. Ferguson, N.H. Miller, G. Li, K.A. Payne, Rabbit model of physeal injury for the evaluation of regenerative medicine approaches, Tissue Eng. C Methods 25 (12) (2019) 701–710.

[26] M. Francesco, S. Roberto, R. Giuliana, F. Filippo, C.D. Andrea, Long term outcome of surgical treatment of chondroblastoma: analysis of local control and growth plate/articular cartilage related complications, BMC Muscoskel. Disord. 24 (1) (2023) 139.

[27] N. Shaw, C. Erickson, S.J. Bryant, V.L. Ferguson, M.D. Krebs, N. Hadley-Miller, K. A. Payne, Regenerative medicine approaches for the treatment of pediatric physeal injuries, Tissue Eng. Part B Rev. 24 (2) (2018) 85–97.

[28] P.T. Newton, L. Li, B. Zhou, C. Schweingruber, M. Hovorakova, M. Xie, X. Sun, L. Sandhow, A.V. Artemov, E. Ivashkin, S. Suter, V. Dyachuk, M. El Shahawy, A. Gritli-Linde, T. Bouderlique, J. Petersen, A. Mollbrink, J. Lundeberg,

G. Enikolopov, H. Qian, K. Fried, M. Kasper, E. Hedlund, I. Adameyko, L. Sävendahl, A.S. Chagin, A radical switch in clonality reveals a stem cell niche in the epiphyseal growth plate, Nature 567 (7747) (2019) 234–238.
[29] S.A. Hallett, Y. Matsushita, W. Ono, N. Sakagami, K. Mizuhashi, N. Tokavanich, M. Nagata, A. Zhou, T. Hirai, H.M. Kronenberg, N. Ono, Chondrocytes in the resting zone of the growth plate are maintained in a Wnt-inhibitory environment, Elife 10 (2021), e64513.
[30] A. Gultekin, Y. Agirdil, B. Oncel Duman, C. Subasi, E. Karaoz, Comparison of mesenchymal stem cell sheets and chondrocyte sheets in a rabbit growth plate injury model, Turk. J. Med. Sci. 50 (4) (2020) 1082–1094.
[31] C.B. Erickson, J.P. Newsom, N.A. Fletcher, Z.M. Feuer, Y. Yu, F. Rodriguez-Fontan, N. Hadley Miller, M.D. Krebs, K.A. Payne, In vivo degradation rate of alginate-chitosan hydrogels influences tissue repair following physeal injury, J. Biomed. Mater. Res. B Appl. Biomater. 108 (6) (2020) 2484–2494.
[32] Y. Han, M. Lian, Q. Wu, Z. Qiao, B. Sun, K. Dai, Effect of pore size on cell behavior using melt electrowritten scaffolds, Front. Bioeng. Biotechnol. 9 (2021), 629270.
[33] K.-S. Han, J.E. Song, N. Tripathy, H. Kim, B.M. Moon, C.H. Park, G. Khang, Effect of pore sizes of silk scaffolds for cartilage tissue engineering, Macromol. Res. 23 (12) (2015) 1091–1097.
[34] S. Nuernberger, N. Cyran, C. Albrecht, H. Redl, V. Vecsei, S. Marlovits, The influence of scaffold architecture on chondrocyte distribution and behavior in matrix-associated chondrocyte transplantation grafts, Biomaterials 32 (4) (2011) 1032–1040.
[35] J.B. Jonnalagadda, I.V. Rivero, J.S. Dertien, In vitro chondrocyte behavior on porous biodegradable poly(e-caprolactone)/polyglycolic acid scaffolds for articular chondrocyte adhesion and proliferation, J. Biomater. Sci. Polym. Ed. 26 (7) (2015) 401–419.
[36] C. Wang, N. Feng, F. Chang, J. Wang, B. Yuan, Y. Cheng, H. Liu, J. Yu, J. Zou, J. Ding, X. Chen, Injectable cholesterol-enhanced stereocomplex polylactide thermogel loading chondrocytes for optimized cartilage regeneration, Adv. Healthc. Mater. 8 (14) (2019), e1900312.
[37] M. Bazgir, M. Saeinasab, W. Zhang, X. Zhang, K. Min Tsui, A. Maasoumi Sarvestani, S. Nawaz, P. Coates, M. Youseffi, J. Elies, F. Sefat, Investigation of cell adhesion and cell viability of the endothelial and fibroblast cells on electrospun PCL, PLGA and coaxial scaffolds for production of tissue engineered blood vessel, J. Funct. Biomater. 13 (4) (2022) 282.
[38] A. Bhaskaran, T. Prasad, T.V. Kumary, P.R. Anil Kumar, Simple and efficient approach for improved cytocompatibility and faster degradation of electrospun polycaprolactone fibers, Polym. Bull. 76 (3) (2018) 1333–1347.
[39] C.S. Moura, J.C. Silva, S. Faria, P.R. Fernandes, C.L. da Silva, J.M.S. Cabral, R. Linhardt, P.J. Bartolo, F.C. Ferreira, Chondrogenic differentiation of mesenchymal stem/stromal cells on 3D porous poly (epsilon-caprolactone) scaffolds: effects of material alkaline treatment and chondroitin sulfate supplementation, J. Biosci. Bioeng. 129 (6) (2020) 756–764.
[40] G. Chen, H.H. Bau, C.H. Li, In situ transmission electron microscope liquid cell 3D profile reconstruction and analysis of nanoscale liquid water contact line movements, Langmuir 35 (51) (2019) 16712–16717.
[41] Y. Kaptan, Y. Guvenilir, Enzymatic PCL-grafting to NH(2)-end grouped silica and development of microspheres for pH-stimulated release of a hydrophobic model drug, Eur. J. Pharm. Biopharm. 181 (2022) 60–78.
[42] M. Azimi, E. Asselin, Improving surface functionality, hydrophilicity, and interfacial adhesion properties of high-density polyethylene with activated peroxides, ACS Appl. Mater. Interfaces 14 (2) (2022) 3601–3609.
[43] Q. Thijssen, L. Parmentier, K. Van Holsbeeck, S. Ballet, S. Van Vlierberghe, Nature-inspired dual purpose strategy toward cell-adhesive PCL networks: C(-linker-)RGD incorporation via thiol-ene crosslinking, Biomacromolecules 24 (4) (2023) 1638–1647.
[44] A.O. Solovieva, N.A. Sitnikova, V.V. Nimaev, E.A. Koroleva, A.M. Manakhov, PRP of T2DM patient immobilized on PCL nanofibers stimulate endothelial cells proliferation, Int. J. Mol. Sci. 24 (9) (2023) 8262.
[45] T. Egghe, S. Aliakbarshirazi, Y. Guo, R. Ghobeira, R. Morent, R. Hoogenboom, N. De Geyter, Comparison of the surface properties and cytocompatibility between plasma activated and homogeneously polydopamine-coated PCL nanofibers as a result of a pre-plasma activation step, Surf. Coating. Technol. 447 (2022), 128808.
[46] L. Berten-Schunk, Y. Roger, H. Bunjes, A. Hoffmann, Release of TGF-beta(3) from surface-modified PCL fiber mats triggers a dose-dependent chondrogenic differentiation of human mesenchymal stromal cells, Pharmaceutics 15 (4) (2023) 1303.
[47] S.K.C. Sundararaj, R.D. Cieply, G. Gupta, T.A. Milbrandt, D.A. Puleo, Treatment of growth plate injury using IGF-I-loaded PLGA scaffolds, J.Tissue Eng. Regenerat. Med. 9 (12) (2015) E202–E209.
[48] X. Ouyang, Y. Xie, G. Wang, Mechanical stimulation promotes the proliferation and the cartilage phenotype of mesenchymal stem cells and chondrocytes co-cultured in vitro, Biomed. Pharmacother. 117 (2019), 109146.
[49] B. Wang, W. Liu, J.J. Li, S. Chai, D. Xing, H. Yu, Y. Zhang, W. Yan, Z. Xu, B. Zhao, Y. Du, Q. Jiang, A low dose cell therapy system for treating osteoarthritis: in vivo study and in vitro mechanistic investigations, Bioact. Mater. 7 (2022) 478–490.
[50] T.W. Kim, M.C. Lee, H.C. Bae, H.S. Han, Direct coculture of human chondrocytes and synovium-derived stem cells enhances in vitro chondrogenesis, Cell J 20 (1) (2018) 53–60.
[51] C. Qing, C. Wei-ding, F. Wei-min, Co-culture of chondrocytes and bone marrow mesenchymal stem cells in vitro enhances the expression of cartilaginous extracellular matrix components, Braz. J. Med. Biol. Res. 44 (4) (2011) 303–310.
[52] J.H. Nam, S.Y. Lee, G. Khan, E.S. Park, Validation of the optimal scaffold pore size of nasal implants using the 3-dimensional culture technique, Arch. Plast Surg. 47 (4) (2020) 310–316.
[53] W. Badar, H. Ali, O.N. Brooker, E. Newham, T. Snow, N.J. Terrill, G. Tozzi, P. Fratzl, M.M. Knight, H.S. Gupta, Collagen pre-strain discontinuity at the bone-Cartilage interface, PLoS One 17 (9) (2022), e0273832.
[54] Y. Zhao, Z. You, D. Xing, J.J. Li, Q. Zhang, H. Huang, Z. Li, S. Jiang, Z. Wu, Y. Zhang, W. Li, L. Zhang, Y. Du, J. Lin, Comparison of chondrocytes in knee osteoarthritis and regulation by scaffold pore size and stiffness, Tissue Eng Part A 27 (3–4) (2021) 223–236.
[55] M. Tanaka, Y. Miyamoto, K. Sasa, K. Yoshimura, A. Yamada, T. Shirota, R. Kamijo, Low oxygen tension suppresses the death of chondrocyte-like ATDC5 cells induced by interleukin-1ss, in Vitro Cell, Dev. Biol. Anim. 58 (7) (2022) 521–528.
[56] W.C. Li, R.J. Xu, J.X. Huang, X. Bao, B. Zhao, Treatment of rabbit growth plate injuries with oriented ECM scaffold and autologous BMSCs, Sci. Rep. 7 (2017), 44140.